Journal of Power Sources 260 (2014) 150–158

Contents lists available at ScienceDirect

Journal of Power Sources

journal homepage: www.elsevier.com/locate/jpowsour

Short communication

Investigation of dynamic driving cycle effect on the degradation of proton exchange membrane fuel cell by segmented cell technology

R. Lin [a,b,*], F. Xiong [a,b], W.C. Tang [a,b], L. Técher [b,c], J.M. Zhang [a,b], J.X. Ma [a,b]

[a] Clean Energy Automotive Engineering Center, 4800 Caoan Road, Tongji University, Shanghai 201804, China
[b] School of Automotive Studies, 4800 Caoan Road, Tongji University, Shanghai 201804, China
[c] Arts et Métiers ParisTech, 151 Boulevard de l'Hôpital, 75013 Paris, France

HIGHLIGHTS

- The effect of driving cycles on the performance of fuel cell was evaluated.
- Segmented fuel cell was used to record the local changes of the current density.
- Mass transport of gases and water could be deduced from the distribution of current densities in different regions.
- Degradation of catalyst layer and Pt particle after driving cycles.
- EDS was adopt to investigate each segment's Pt distribution.

ARTICLE INFO

Article history:
Received 21 November 2013
Received in revised form
24 February 2014
Accepted 1 March 2014
Available online 15 March 2014

Keywords:
Proton exchange membrane fuel cell
Driving cycles
Degradation
Segmented cell technology

ABSTRACT

Durability is one of the most important limiting factors for the commercialization of proton exchange membrane fuel cell (PEMFC). Fuel cells are more vulnerable to degradation under operating conditions as dynamic load cycle or start up/shut down. The purpose of this study is to evaluate influences of driving cycles on the durability of fuel cells through analyzing the degradation mechanism of a segmented cell in real time. This study demonstrates that the performance of the fuel cell significantly decreases after 200 cycles. The segmented cell technology is used to measure the local current density distribution, which shows that the current density at the exit region and the inlet region declines much faster than the other parts. Meanwhile, electro-chemical impedance spectroscopy (EIS) reveals that after 200 cycles the ohmic resistance of fuel cell increases, especially at the cathode, and electro-chemical surface area (ESA) decreases from 392 to 307 cm^2 mg^{-1}. Furthermore, scanning electron microscopy (SEM) images of the membrane–electrode assembly (MEA) in cross-section demonstrate crackle flaw on the surface of the catalyst layer and the delamination of the electrodes from the membrane. Transmission electron microscope (TEM) results also show that the Pt particle size increases distinctly after driving cycles.

1. Introduction

Proton exchange membrane fuel cell (PEMFC) is one of the promising types of fuel cells that can be used as a vehicular power source to replace gasoline and diesel internal combustion engine. However, there are still many obstacles to be overcome before commercialization, including concerns about the high cost and low durability. According to the standard released by American Department of Energy, the life time of a PEMFC system in a vehicle operated under real-world conditions is expected to get to 5000 h with less than 10% degradation, while currently it is no more than 2500 h [1].

The performance of fuel cell is prone to material degradation. A variety of tests were conducted at a stationary condition. The purpose of these tests was to provide an overview of the effect of operating conditions, including the effects of reactant gas flows, humidification levels and temperatures on the fuel cell performance and the corresponding morphological change of single fuel cells [2]. However, comparatively to dynamic driving cycles, the steady-state operating condition is more time-consuming. Also, the performance of a vehicle in a stationary condition is significantly different from the performance in a real working condition [3]. Comparatively to the steady condition under the constant load, the

* Corresponding author. Clean Energy Automotive Engineering Center, 4800 Caoan Road, Tongji University, Shanghai 201804, China.
E-mail address: ruilin@tongji.edu.cn (R. Lin).

http://dx.doi.org/10.1016/j.jpowsour.2014.03.003
0378-7753/

operating condition of the dynamic driving cycles changes much more dramatically. This may result in oxidant starvation, local hotspots and physical degradation. Therefore, the performance of the cell would be seriously degraded [4].

To determine the durability and performance of fuel cells, several researches have proposed and implemented different dynamic load cycles. For instance, Borup and Mukundan [5] conducted the dynamic durability test using a modified US06 driving cycle to vary the power output. Results of Borup's study show that the degree of particle size growth is dependent upon the amount of water in the fuel cell. Tang [6] applied a driving cycle including open circuit, idle condition, rated condition and overload condition, which took 430 min per cycle. They also compared the degradation rate between high Pt loads and low Pt loads. The above-mentioned studies show that the membrane has been seriously degraded but fail to highlight the inhomogeneity of degradation on different regions of the membrane.

To investigate the degradation mechanism of fuel cells, this study adopted the same driving cycles as described in R. Lin's previous paper [7]. The printed circuit board (PCB) technology was introduced in this study to measure the local current density distribution and to examine the changes of local electro-chemical reaction in the degradation process. In addition, scanning electron microscopy (SEM) and transmission electron microscopy (TEM) were used in this study to investigate the microstructure degradation mechanism of fuel cell materials.

2. Experiment

2.1. Preparation of membrane–electrode assembly (MEA)

Membrane–electrode assemblies purchased from Wuhan Xinyuan Corporation were used in this experiment [8]. Anodic catalyst and catholic catalyst with 0.4 mg cm^{-2} Pt obtained from Johns Manville Corporation were coated on the membrane. The membrane thickness was 23 μm. The effective electrode area was 50 cm^2. The characteristics of the MEA have been previously introduced [9].

2.2. Description of test conditions and dynamic driving cycles

The cell temperature was maintained at 80 °C. Back pressures of anode and cathode were kept at 0.2 bar. Both anode and cathode sides were 100% humidified by external humidifiers. Table 1 shows the applied operating conditions. Hydrogen stoichiometry (λ_{H_2}) and air stoichiometry (λ_{Air}) were kept constant at 1.2 and 2.5, respectively. The three channel serpentine flow field was applied to both the anode and the cathode sides of the cell. In order to keep the MEA, the gaskets and the PCB in good contact, clamping pressure of 8 bar was provided by cylinder compression.

Table 1
Operating conditions.

Anode reactant gas	Hydrogen	99.99%
	Humidity	100%
	λ_{H_2}	1.2
Cathode reactant gas	Air	99.99%
	Humidity	100%
	λ_{Air}	2.5
Clamping	Cylinder compression force	8 bar
Backing pressure	Anode	0.2 bar
	Cathode	0.2 bar
Cell temperature		80 °C

The dynamic driving cycles were designed by simulating the real internal engine vehicle with consideration about idle running, constant load running, variable load acceleration, full power running and overload running. Each cycle lasted for 20 min, as referenced to our previous work [6]. The rated loading and overloading were set respectively at 45 A and 50 A. The evolution of current and voltage in one cycle is presented in Fig. 1a and b, respectively. Due to membrane failure, the aging tests were stopped after 200 cycles. In order to eliminate the effects of the start-up phase on the performance of the cell, nitrogen was passed through the anode and the cathode before air and hydrogen were passed through the electrodes. After periodic driving cycles, the performance of the cell was recorded, using methods of the *I–V* curve, electro-chemical impedance spectroscopy (EIS), cyclic voltammetry (CV), etc. The current density distributions were recorded during the whole testing process.

2.3. I–V curves

Fig. 1b demonstrates the transient voltages response to current densities. The changes of the transient voltage as the evolution of every driving cycle cannot be used to illustrate the degradation of fuel cells. Therefore, for presenting the degradation of the cell the polarization curve of the cell must be recorded. *I–V* curves were measured under the same operating condition, when the cell was activated, and operated after 100, 150 and 200 cycles, respectively.

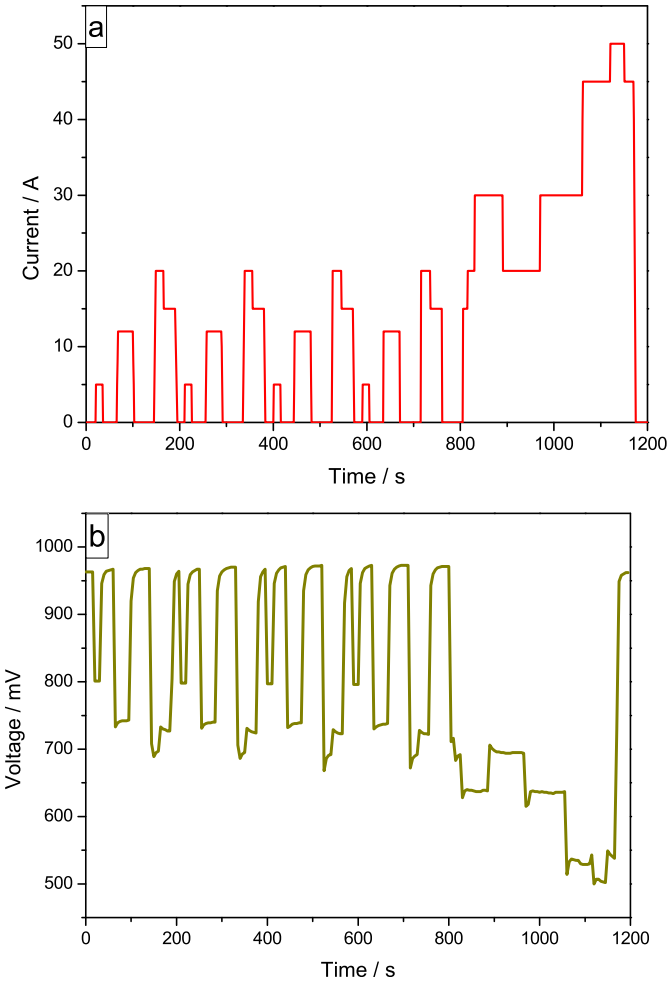

Fig. 1. Evolution of current (a) in a simulate driving cycle and response voltage (b) in one cycle.

Before the polarization tests were performed, the cell was operated in steady-state condition for 20 min, which helped to avoid any impact from recent chronological account of the characterization measurements [10].

2.4. Electro-chemical impedance spectroscopy

The electro-chemical impedance spectroscopy (EIS) of the cell was performed to investigate the following: the internal property of MEA, including ohmic resistance, charge transfer resistance for the oxygen reduction, mass transfer resistance of oxygen in the catalyst layer, and constant phase element of the catalyst layer capacitance. EIS measurements of the cell were carried out using a VMP2/Z workstation by a PAR model at galvanostatic mode. It was done under a constant load of 4.5 A with a frequency range from 100 mHz to 10 kHz. All impedance spectra reported herein were measured between cathode and anode sides of the cell. Air was passed through the test electrode while hydrogen was passed through the counter electrode. Due to the negligible over-potential for hydrogen oxidation and reduction on platinum catalyst, the counter electrode was also used as the reference electrode.

2.5. Cyclic voltammetry

Cyclic voltammetry (CV) measurement was conducted to calculate the electro-chemical surface area of MEA. As the electro-chemical surface area (ESA) of cathode was measured, nitrogen was passed through the cathode, which was set as the test electrode. Hydrogen was passed through the anode, which was set as the reference electrode. After the open circuit voltage (OCV) decreased to 100 mV or below, the potential was scanned from 50 mV to 1100 mV versus the reversible hydrogen electrode (RHE) at a rate of 20 mV s^{-1}. ESA was evaluated from the CV by dividing the charge (μC) that corresponded to the area under the hydrogen desorption region by 210 μC. The equation is the following:

$$Se = \frac{0.1 \times Q_r}{m \times c}$$

where Se is the ESA, Q_r is the integral area of hydrogen oxidation desorption peak in CV curve, m is the loading of platinum, and c is the electrical charge associated with monolayer adsorption of hydrogen on Pt surface [11].

2.6. Segmented cell technology

For the measurement of current density distribution, the printed circuit board (PCB) approach was adopted. Based on PCB technology, we segmented the bipolar plate with the method introduced in R. Lin's paper [7]. The segmented bipolar plate integrated with temperature sensors was put between MEA and anode current collector plate. It aimed to reduce the effect of PCB on the operational behavior of the cell. Temperature distribution of the cell was measured by temperature sensors in local regions. The effects of PCB on accuracy of measurement results depended on the ratio of in-plane to out-of-plane electronic conductivity of electrodes, gas diffusion layers, and bipolar plates. The coupling of the current density distribution at the anode and the cathode was found by R. Lin's work, which can verify that the effects of the insertion of the PCB can be ignored [12]. The current density data of every segmented cell was collected by Agilent 34970A device, and presented by the seglab software. The experimental parameters, controllers and measuring devices are summarized in Table 2 [13].

Table 2
Measurement uncertainties.

	Source	Range	Error
Gas mass flow controller	Alicat scientific		
Anode (H_2)		1 SLPM	±1% of full scale
Cathode (air)		2 SLPM	±1% of full scale
Cell temperature	Xiamen Yudian		±1 °C
Electronic load	KIKUSUI PLZ-4W	50 V/150 A	
Constant current (CC)		150 A	±0.3% of full scale
Constant voltage (CV)		50 V	±0.2% of full scale
Data logger	Aglient 34970A		
DC voltage		100 mV	±6.5 μV
		1 V	±26 μV
		10 V	±190 μV

2.7. Scanning electron microscopy (SEM)

SEM micrographs of the catalyst layers were examined by the JSM-5600LVSEM device to investigate the effects of dynamic driving cycles on the microstructure of the electrode, including the changes in the catalyst layer surface and its cross-section, as well as the change of catalyst particles distribution. By comparing the MEA operated after dynamic driving cycles with the fresh MEA, the microstructure changes of the MEA could be found. Also, the Energy Dispersive Spectrometer (EDS) mapping of the MEA of different regions was investigated to show the distribution of different elements.

2.8. Transmission electron microscopy (TEM)

To investigate the degradation of the catalyst, TEMs of the cathode and anode catalyst were examined by JEM 2010EX microscope, operating at 200 kV. Cu-*Ka* radiation was employed. The structure of the Pt/C catalyst was examined using the HR-TEM technique. In addition, the particle size of Pt and its distribution were analyzed.

3. Results and discussion

3.1. Effects of dynamic cycles on single cell performance

In order to investigate the effect of dynamic cycles on the performance of the MEA, polarization curves at fresh, 100, 150 and 200 cycles are recorded as shown in Fig. 2. It is found that after dynamic

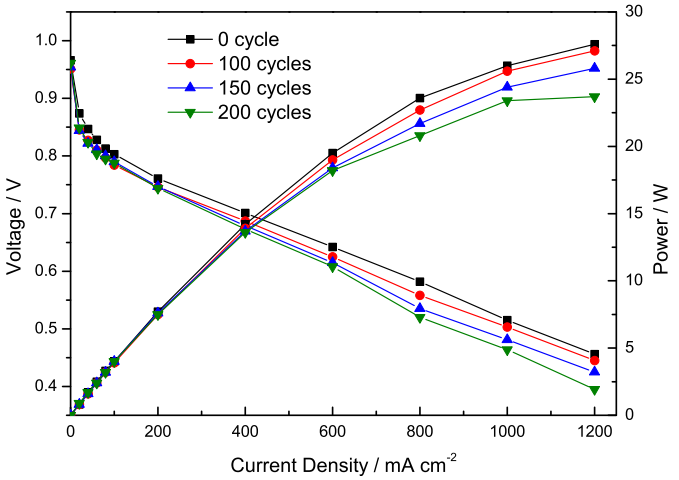

Fig. 2. Polarization curves of fresh MEA and those measured after 100, 150 and 200 cycles.

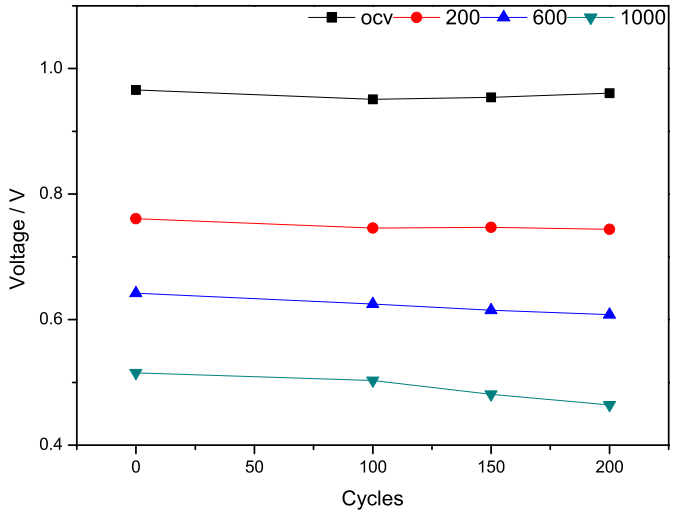

Fig. 3. Average decline rate of voltage after driving cycles, respectively at 0, 200, 600, 1000 mA cm^{-2}.

cycles the OCV doesn't have an apparent deviation, while at 1200 mA cm^{-2} the voltage decreases rapidly. This phenomenon could also be detected from the average decline rate of voltage at different current density (Fig. 3). At low current density regions (lower than 200 mA cm^{-2}), the response voltage of the cell does not apparently decrease. However, at high current density, such as 1000 mA cm^{-2}, the voltage decreases obviously from 0.515 to 0.464 V. The average decline rate of voltage is 225 μV per cycle. It demonstrates that at high current density, the decline rate of performance is much higher than that at the low current density. It is due to the mass transfer limitation at high current density.

3.2. CV and EIS measurement

CV curves after driving cycles are presented in Fig. 4. They are applied to investigate the effects of the driving cycles on the electro-chemical active area. ESA of the catalyst is calculated from the CV data, and is presented in Fig. 5. It is found that the area of hydrogen adsorption decreases after the driving cycles. Specifically after 100, 150 and 200 cycles, the ESA of cathode catalyst decreases

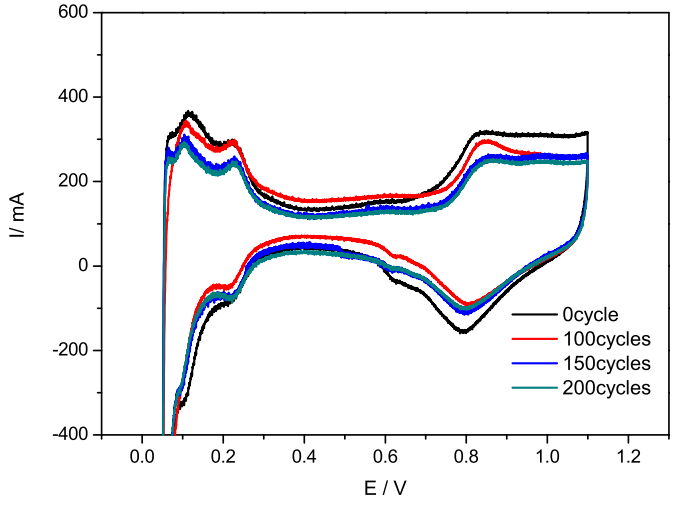

Fig. 4. Cyclic voltammetry (CV) curves of fresh MEA and those measured after 100, 150 and 200 cycles.

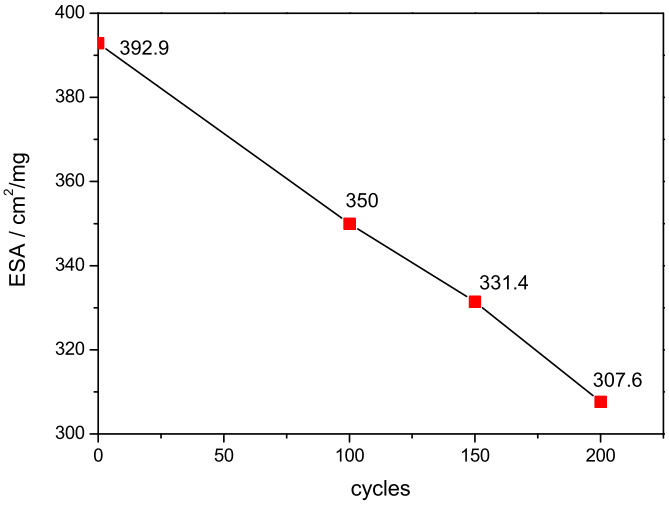

Fig. 5. Electro-chemical surface area (ESA) of cathode catalyst after activated, 100, 150 and 200 cycles.

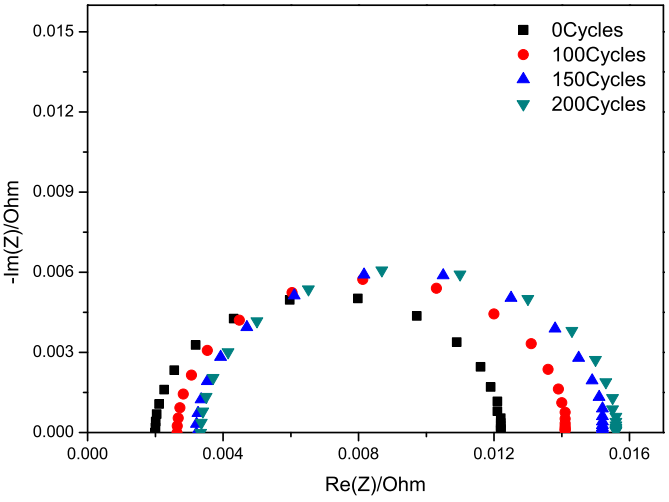

Fig. 6. Electro-chemical impedance spectroscopy (EIS) of fuel cell after driving cycles (fresh, 100, 150 and 200 cycles).

respectively from 392.9 to 350, 331.4 and 307.6 cm^2 mg^{-1} with a dropping rate of 0.43 cm^2 mg^{-1} per cycle.

Analysis of results that are presented in Figs. 2 and 3 demonstrates that the electro-chemical active area of catalyst decreases

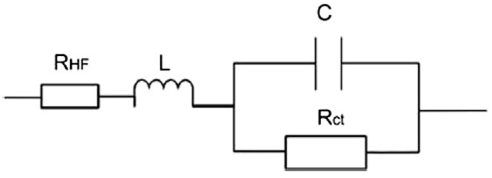

Fig. 7. Equivalent circuit for impedance analysis.

Table 3
Results of equivalent circuit for the impedance analysis.

Driving cycles	0	100	150	200
L e-07 (H cm^2)	0.63	8.93	1.25	1.25
R_{HF} (mΩ cm^2)	1.96	2.63	3.19	3.32
CF cm^{-2}	1.15	0.85	0.63	0.59
Rct (mΩ cm^2)	10.21	11.5	12.05	12.27

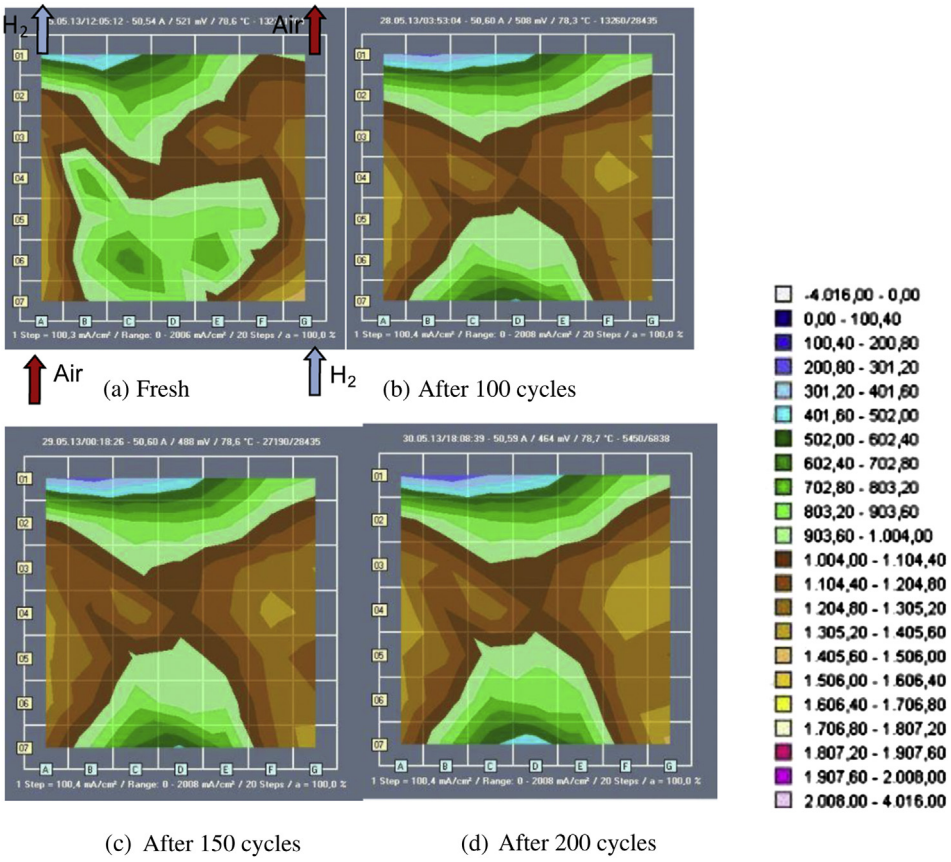

Fig. 8. Current density distribution at 1000 mA cm^{-2} after driving cycles (0, 100,150 and 200 cycles).

after driving cycles. At low current density, the demand of the electro-chemical reaction active area is not high. However, at high current density, MEA could not provide enough active sites for electro-chemical reaction. It results in a very obvious performance reduction of the cell at 1000 mA cm^{-2} [14].

The performance of the fuel cell has a significant correlation with the electro-chemical impedance. The conductivity of the electron and proton in the cathode catalyst layer has a significant impact on the reduction of the oxygen at cathode side. Therefore, EIS of the cell operated under dynamic driving cycles was recorded after 0, 100, 150 and 200 cycles, as shown in Fig. 6. At the beginning of the dynamic cycles, a depressed semicircle from EIS plots could be recognized. With continuation of the cycles from 0 to 100 cycles, the real and the imaginary parts of the impedance plots increase at the same time. However, from 100 to 200 cycles, the real parts and the diameter of the loop don't increase obviously.

Equivalent circuit (Fig. 7) is adopted to analyze the impedance. We calculate the R_{HF}, Rct and CPE through the equivalent circuit on the basis of the Nyquist curve, as shown in Table 3. R_{HF} is the ohmic resistance, which contains the ohmic resistance of membrane, catalyst layer and diffusion layer etc.; Rct is the charge transfer resistance of the oxygen reduction reaction, which corresponds to the diameter of the kinetic loop in the Nyquist curve. The capacitance of equivalent circuit depends on the catalyst layer properties associated with the oxygen reduction reaction [15]. As shown in Table 2, the ohmic resistance and the charge transfer resistance of fuel cell increase as driving cycles running, while the capacitance of the cell decreases, which leads to the performance degradation of the cell, as shown in the *I–V* curve.

The polarization curve of Fig. 1 reveals the following three distinguishable regions: an exponential voltage drop at low current densities, which correlates with reaction activation losses, especially at the cathode; a linear decrease of voltage associated with the dominance of the ohmic resistance of the cell at intermediate current density; and a deviation from linear voltage change with a sharper voltage drop at higher current densities due to mass-transport losses. However, for polarized cells, all three voltage loss mechanisms (reaction activation, ohmic, and mass-transport-limited) exist at all currents. The extent of one mechanism dominating the cell behavior (but not necessarily dominating the cell voltage loss) depends on current density and determines the shape of the polarization curve in that region [16]. Based on the analysis of the EIS curves and the equivalent circuit, we find that the Rct mainly affects the low current density, and increases by 20% with the continuation of cycles, from 10.21 to 12.27 mΩ cm^2. The R_{HF} mainly affects the intermediate current density, and increases from 1.96 to 3.32 mΩ cm^2 (70% increase) as cycles going. It is demonstrated that the resistance increases more rapidly at intermediate current density than at low current density. It also explains why the voltage decreases more rapidly at 1000 mA cm^{-2} than at 100 mA cm^{-2}.

3.3. Current density distribution

In order to investigate the local current density distribution and explore the degradation mechanism of the fuel cell, the segmented cell technology is adopted in this experiment. A segmented bipolar plate with 49 segments for a single cell is used in the experiment. The area of every segment is about 1.02 cm^2. Fig. 8 shows that G7

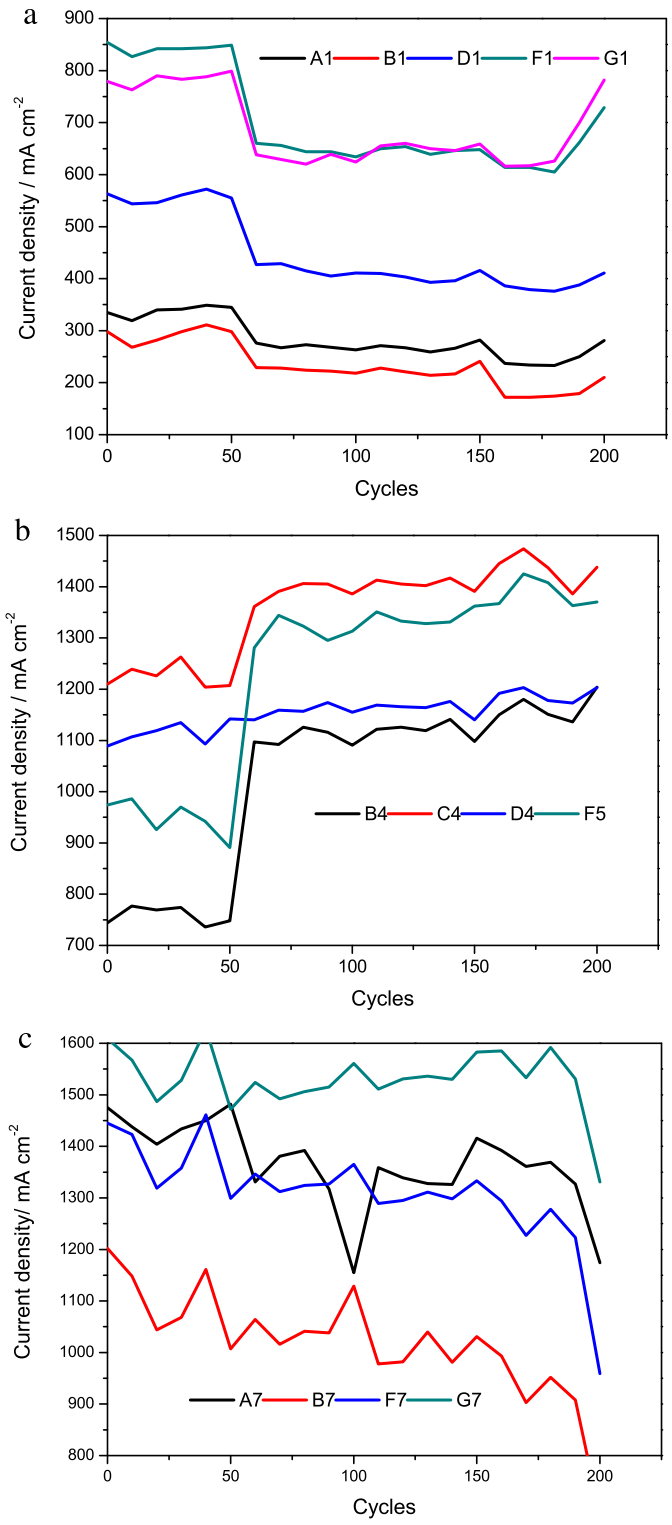

Fig. 9. Changes of the current density in various areas at 1000 mA cm^{-2}: (a) reaction outlet area, (b) middle area of MEA, and (c) reaction inlet area.

and A7 segments are the inlet of hydrogen and air, respectively, and the segment A1 and G1 are the outlet of hydrogen and air, respectively. The cell is operated at 1000 mA cm^{-2}. Different colors (in the web version) stand for different current density values, as is shown by the legend. It shows that at the beginning of the driving cycles, the current density is not evenly distributed. The homogeneity calculated from the span of 20% range of average current density is only 60.3% and the response voltage is 0.621 V. After 100, 150 and 200 driving cycles, the homogeneity decreases to 54.8%, 52.6% and 44.4% respectively, and the response voltage decreases to 0.508, 0.488 and 0.464 V, respectively. During this time the degradation of the fuel cell performance is observed.

The color (in the web version) of D1 and D7 has changed from green (in the web version) to blue (in the web version), which indicates a decrease of the current density at D1 and D7. It could be caused by the degradation of the catalyst of these segments. As the fuel cell remains at the galvanostatic mode, the current density of some segments has to increase to keep the average current density the same. As demonstrated in Fig. 8, the value of the current density of the segments in the middle of the cell, such as segment C3 and D4, increases. As driving cycles running, different regions of the MEA have declined to different extents. It might be due to the reason that though the value of the current density of some segments increases, in other segments it decreases (Fig. 9).

In order to find the pattern of the current density distribution changes, the current density of different areas on the MEA is investigated. It is found that at the outlet and inlet parts of the MEA, the performance drops by 45.4% and 24.3%, respectively. At the same time in the middle region of the MEA, the current density increases. It could be concluded that the segments at the exit and inlet parts of the flow field decline more seriously than those in the middle. At the inlet of the flow field, the flow rate of reaction is very high. It carries the produced water away, leading to the drying of the MEA, which might be the reason for the degradation of the MEA [17]. At the hydrogen outlet, when the load increases, the reaction flow rate does not respond in time, which might lead to starvation of gases [18]. At the air outlet, as the relative humidity increases to 100%, cathode flooding might occur. It could block the flow channels and the pores of the gas diffusion layer (GDL), and aggravate the degradation of MEA [19].

3.4. SEM analysis of MEA after operated under driving cycles

The morphology of the catalyst layer is analyzed using scanning electron microscopy (SEM) technology. It aims to explain a significant decrease of fuel cell performance. Fig. 10a illustrates the SEM result of the MEA at cathode side after activated and Fig. 10b illustrates the SEM result of the MEA at cathode side after 200 cycles. As demonstrated in Fig. 10a, the surface of catalyst layer of the fresh MEA is very smooth, and the Pt/C catalyst is uniformly dispersed. Much bigger pores and highly textured structure are formed in the catalyst layer. After 200 cycles the surface becomes rough (Fig. 10b). The width of the catalyst layer band becomes uneven and much smaller than that of the fresh MEA. Meanwhile, it is shown that after 200 cycles the size and distribution of the particles on the surface change unevenly. Open pores in the catalyst layer are produced to reduce contact resistance between the catalyst layer and the membrane. However, with cycles running, the number of open pores decreases, and the size of the open pores becomes smaller. This is the main reason for the increase of ohmic resistance [20].

Fig. 11 shows the cross-section of the fresh MEA and the aged MEA after 200 cycles. Anode side is located below the membrane. As demonstrated in Fig. 11a, the catalyst is uniformly distributed and the membrane is smooth with no cavities and cracks. However, after 200 cycles, the thickness of the membrane increases from 22.9 to 26.3 μm as the MEA expands. In the same time the structure of the catalyst layer visibly changes, especially for the cathode catalyst layer. Fig. 11b demonstrates development of separations between cathode/anode catalyst layer and membrane (as shown in red circle (in the web version)). Also, it shows that the original texture uniformity of the catalyst layer completely disappears, leaving behind rough structure and portions with different sizes. The MEA has a

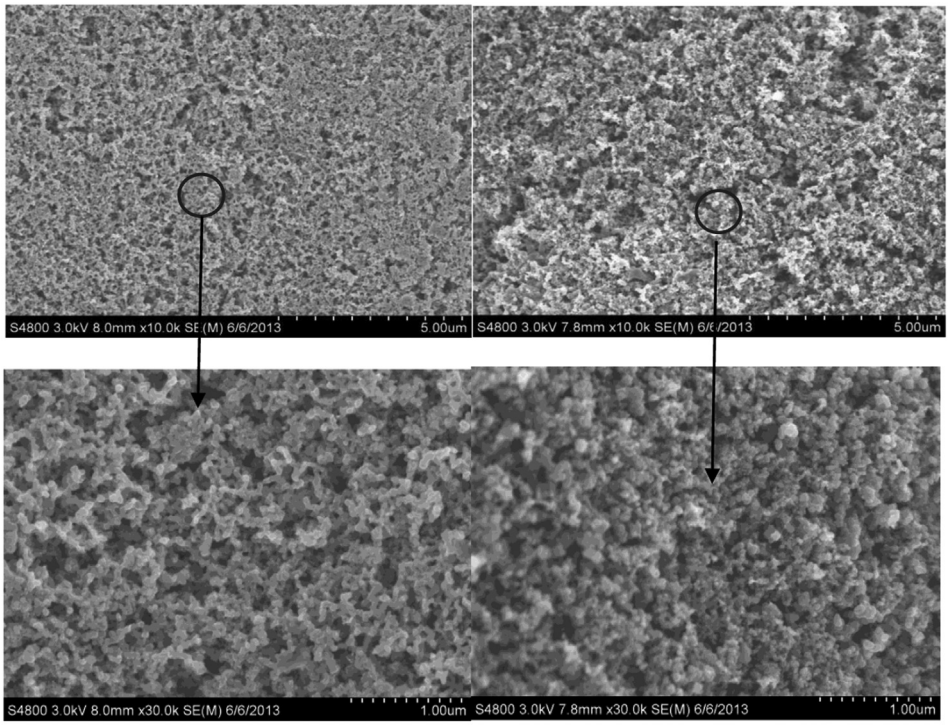

Fig. 10. Scanning electron micrograph (SEM) of the surface layer of catalyst (cathode side).

marked distortion. In summary, a comparative analysis of Fig. 11a and b demonstrates that the driving cycles have a remarkable influence on MEA morphology. Apparently the degradation of the cathode catalyst layer is more serious than the degradation of the anode catalyst layer. According to R. L. Borup's research, the changes of the structure of the cathode catalyst layer might be due to carbon corrosion [21]. The fuel cell operating at 0.9 V accounts for 50% of the corrosion [22]. Meanwhile, when the load becomes high suddenly, the fuel feeding could not respond in time, which may lead to local fuel starvation. These factors could be the main reasons of carbon corrosion. In addition, large amount of water produced from the cell reaction at the cathode might also be a main cause of the cathode degradation. The possible reaction mechanism is as follows:

$$C + 2H_2O = 4H^+ + 4e^- + CO_2$$

$$4H^+ + O_2 + 4e^- = 2H_2O$$

Fig 12 shows results of Energy Dispersive Spectrometer (EDS) measurement of MEA from different regions. Blue (in the web version) points represent Pt element. It demonstrates that Pt elements are sparsely dispersed on the surface of fresh MEA, while Pt elements of degraded MEA are distributed unevenly. Also, the amount of Pt elements has reduced significantly, particularly in D1 and G7 segments. Comparison of Fig. 12(c) and (d) demonstrates apparent Pt particle loss at the cathode. It might lead to the reduction of ESA. Also, it might be one of the reasons why the performance of D1 and G7 segments declines. However, since the Pt particles mainly agglomerate, there is little Pt particles loss concerning the whole MEA (Fig. 13).

3.5. TEM analysis

It is known that the catalyst layer is the most important region for the electro-chemical reaction. The performance of the catalyst significantly affects the speed of the electro-chemical reaction.

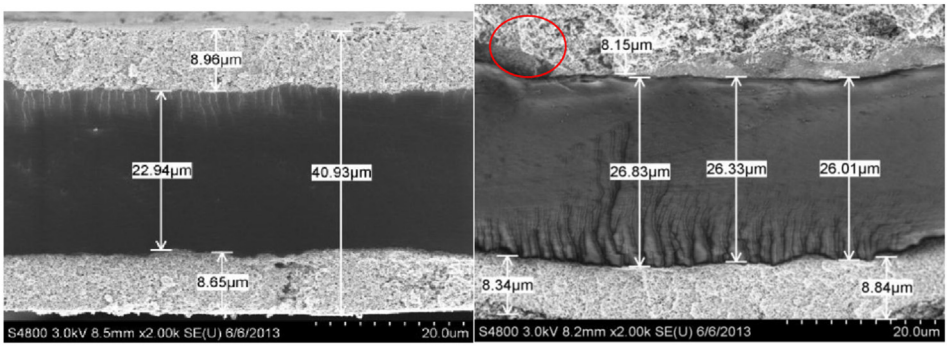

Fig. 11. Cross-section of MEA morphology.

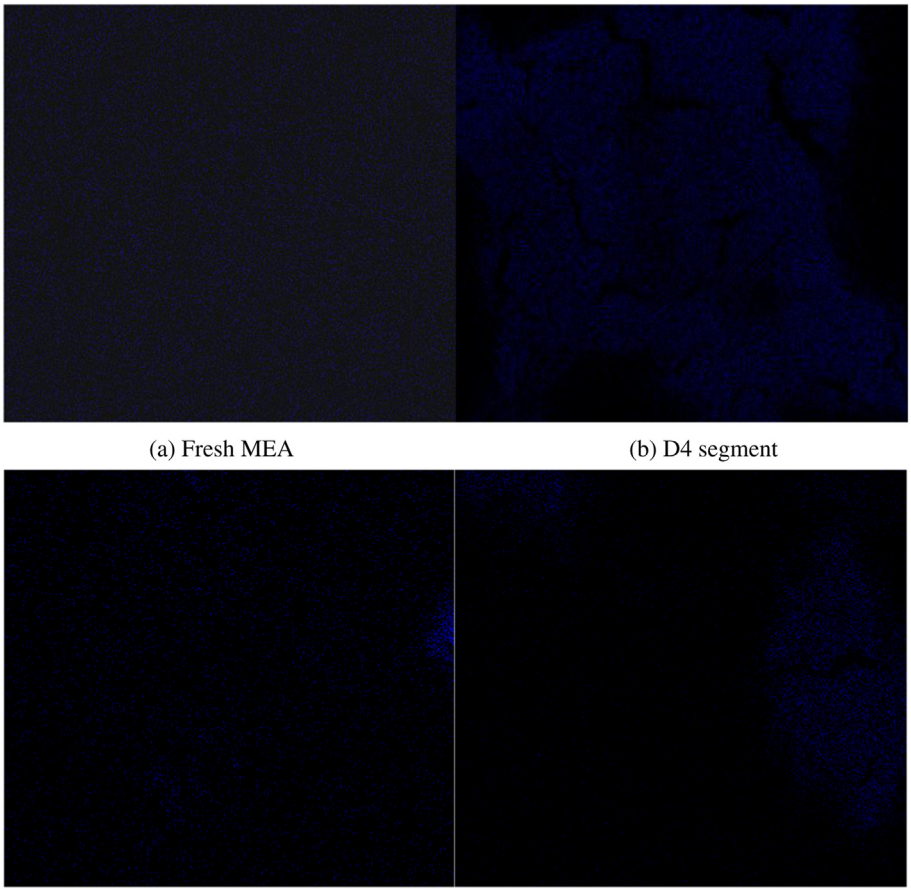

Fig. 12. EDS mapping of MEA from different regions (Pt La1).

Therefore, the catalyst at the cathode and anode, fresh and after driving cycles, is tested by TEM that aims in assessment of the catalyst degradation (Fig. 12). As shown in Fig. 12a, Pt particles are uniformly dispersed on the carbon carrier. It can be seen from Fig. 12b and c that, after 200 driving cycles, the Pt particles distribution of the cathode becomes very uneven, and the Pt particles of the cathode grow up obviously. According to Wang's research [23], when the potential is set between 0.65 V and 1.1 V, the dissolution rate of Pt particle would increase with the increase of the potential. It probably may explain that the growing up of the catalyst particles could be mainly due to high potential at the cathode side. After the dissolution of Pt, the reaction is as follows:

$$Pt \rightarrow Pt^{4+} + 4e^{-}, \quad PtO_2 + 4H^{+} \rightarrow Pt + 2H_2O$$

Meanwhile, it is also found that the amount of Pt particles at the cathode decreases, which might be due to the migration of Pt particle. This also causes the degradation of the catalyst.

4. Conclusions

In this paper, driving cycles are designed in a way that simulates operation conditions of the real vehicle. The performance and microstructure of the fuel cell after 100, 150 and 200 cycles are tested. The cell voltage decreases at a rate of 225 μV per cycle under

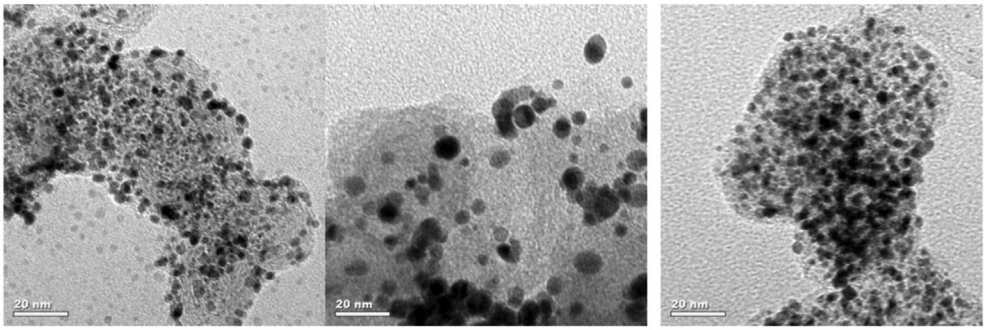

Fig. 13. Transmission electron microscope (TEM) micrographs of catalyst.

constant current density of 1000 mA cm^{-2}. It is shown that the performance degrades more quickly when the cell is loaded with high current density. The ohmic resistance and active resistance of cathode increase from 1.96 to 3.32 mΩ cm^2 and 10.21 to 12.27 mΩ cm^2, respectively. After 200 driving cycles the electrochemical active area decreases from 392 cm^2 mg^{-1} (fresh MEA) to 307.6 cm^2 mg^{-1}. These results in combination with CV and EIS results clearly indicate the degradation of MEA.

SEM results demonstrate significant changes of the surface and cross-section of the catalyst layer. Also, the open pores on the catalyst layer become smaller and unevenly distributed. The cathode catalyst layer becomes distorted. Furthermore, TEM results demonstrate that Pt particles grow up obviously, which decreases the activity of the catalyst.

Meanwhile, after 200 cycles, the current density of the segments at the inlet and outlet of the flow field decreases by 24.3% and 45.4% respectively with a constant average current density of 1000 mA cm^{-2}. At the same time the current density in the middle regions increases. Based on analysis of the local current density distribution, it might be concluded that the MEA at the inlet and exit of the flow field declines more seriously than that in the middle.

Overall, this study demonstrates that dynamic driving cycles significantly impact the performance of fuel cell. The segmented cell technology aims in investigating the local current density distribution. It provides knowledge about the degradation of MEA at different regions, which helps to understand the degradation mechanism.

Acknowledgment

The authors gratefully acknowledge the financial support from National Natural Science Foundation of China (_501100001809) (No. 21276199, No. 21310102016), The Young Talents “Climbing” Program of Tongji University, National Key Scientific Instrument and Equipment Development Special Fund (2012YQ150256), The Fundamental Research Funds for the Central Universities and 111 Project (No. B08019).

References

[1] http://www.eere.energy.gov/hydrogenandfuelcells/accomplishments.html.
[2] M. Schulze, T. Knöri, A. Schneider, E. Gülzow, J. Power Sources 127 (2004) 222.
[3] A. El-kharouf, A. Chandan, M. Hattenberger, B.G. Pollet, J. Energy Inst. 85 (2012) 188.
[4] X.Q. Yan, M. Hou, L.Y. Sun, H.B. Cheng, Y.L. Hong, D. Liang, J. Power Sources 163 (2007) 966.
[5] R.L. Borup, R. Mukundan, ECS Trans. 33 (2010) 17.
[6] J.J. Tang, Master thesis, Wuhan University of Technology, 2011.
[7] R. Lin, B. Li, Y.P. Hou, J.M. Ma, Int. J. Hydrogen Energy 34 (2009) 2369.
[8] http://www.wutenergy.com/1.asp.
[9] W.C. Tang, R. Lin, Y.M. Weng, J.M. Zhang, J.X. Ma, Int. J. Hydrogen Energy 38 (2013) 10985.
[10] B. Wahdame, D. Candusso, F. Harel, X. François, M.-C. Péra, D. Hissel, J.-M. Kauffmann, J. Power Sources 182 (2008) 429.
[11] T.R. Ralph, G.A. Hards, J.E. Keating, J. Electrochem. Soc. 144 (1997) 3845.
[12] R. Lin, E. Gülzow, M. Schulze, K.A. Friedrich, J. Electrochem. Soc. 158 (2011) B11.
[13] R. Lin, C.H. Cao, J.X. Ma, E. Gülzow, K.A. Friedrich, Int. J. Hydrogen Energy 37 (2012) 3373.
[14] J.R. Yu, T. Matsuura, Y. Yoshikawa, M.N. Islam, M. Hori, Electrochem. Solid State Lett. 8 (2005) A156.
[15] A. Fischer, J. Jindra, H. Wendt, J. Appl. Electrochem. 28 (1998) 277.
[16] D. Malevich, E. Halliop, B.A. Peppley, J.G. Pharoah, K. Karan, J. Electrochem. Soc. 156 (2009) B216.
[17] S.S. Zhang, X.Z. Yuan, H.J. Wang, W. Mérida, H. Zhu, J. Shen, S.H. Wu, J.J. Zhang, Int. J. Hydrogen Energy 34 (2009) 388.
[18] L. Guétaz, S. Escribano, O. Sicardy, J. Power Sources 212 (2012) 169.
[19] W. Schmittinger, A. Vahidi, J. Power Sources 180 (2008) 1.
[20] B. Li, R. Lin, D.J. Yang, J.X. Ma, Int. J. Hydrogen Energy 35 (2010) 2814.
[21] D. Sperniak, J. Fairweather, R. Mukundan, T. Rochward, R.L. Borup, J. Power Sources 214 (2012) 386.
[22] K. Panha, M. Fowler, X.-Z. Yuan, H.J. Wang, Appl. Energy 93 (2012) 90.
[23] X. Wang, R. Kumar, D.J. Myers, Electrochem. Solid State Lett. 9 (2006) A225.